Impact of glacially induced stress changes on fault-seal integrity offshore Norway

Balz Grollimund and Mark D. Zoback

ABSTRACT

In this study, we use a three-dimensional numerical model of glacially related lithospheric flexure to estimate in-situ stress and pore pressure changes through time in the Norwegian sector of the northern North Sea. The model results match available borehole measurements of in-situ stress and pore pressure, which show a transition from high horizontal stresses at large distances from the coast to lower horizontal stresses in near-coastal areas and an associated rotation in stress orientation. In addition to the present-day predictions, the model results provide an estimate for the evolution of stress and pore pressure during glacial and interglacial periods. We found that the temporally changing stress field might have induced repeated reactivation of reservoir-bounding faults during the course of the Pleistocene glaciations, especially during Weichselian interglacials. As a result, hydrocarbon fields in the Norwegian offshore areas appear to have been exposed to multiple periods of fault reactivation and potential hydrocarbon leakage.

INTRODUCTION

Extensive numerical modeling suggests that lithospheric bending, because of the Pleistocene glaciations, is a major source of lateral stress variations in the northern North Sea and on the mid-Norwegian margin. According to the modeling, which will be presented subsequently, the complicated ice sheet geometries (Figure 1) are mainly responsible for the observed present-day pattern of stress orientations and magnitudes in the area. In this paper, we first study the present-day model prediction and compare them to in-situ stress observations. In a second step, we will utilize the model results to track stress changes with time and to predict the impact of stress changes related to ice sheet advances and retreats on selected hydrocarbon reservoirs.

Several processes related to the Pliocene–Pleistocene glacial period could have affected hydrocarbon reservoirs along the Norwegian

Copyright ©2003. The American Association of Petroleum Geologists. All rights reserved.

Manuscript received November 16, 2001; provisional acceptance April 30, 2002; revised manuscript received July 20, 2002; final acceptance August 1, 2002.

AUTHORS

BALZ GROLLIMUND ~ *Geomechanics International, 250 Cambridge Avenue, Suite 103, Palo Alto, California 94306*

Balz Grollimund is working as a geomechanical consultant for Geomechanics International. He received a diploma (equivalent to M.S. degree) in structural geology from ETH in Zurich, Switzerland in 1996 and his M.S. degree and Ph.D. in geophysics from Stanford University in 1999 and 2000, respectively. During his Ph.D. in the stress and crustal mechanics group of Mark Zoback, he was studying the in-situ state of stress offshore Norway and its implications for fault-seal integrity.

MARK D. ZOBACK ~ *Department of Geophysics, Stanford University, Stanford, California 94305*

Mark Zoback is professor of geophysics in the School of Earth Sciences at Stanford University. He received his B.S. degree in geophysics from the University of Arizona in 1969 and his M.S. degree and Ph.D. from Stanford in 1973 and 1975, respectively. From 1975 to 1984, he worked at the U.S. Geological Survey in the Office of Earthquake Studies. His principal scientific interests are related to the state of stress in the Earth's crust and the mechanics of crustal faulting.

ACKNOWLEDGEMENTS

We thank Norsk Hydro for generously providing the data and financial support for this study and David Wiprut for very helpful information on current leakage in the Visund, Field 3, and Field 1. We also thank Russell Davies, Scott Young, and Donald Medwedeff for their constructive reviews of the manuscript.

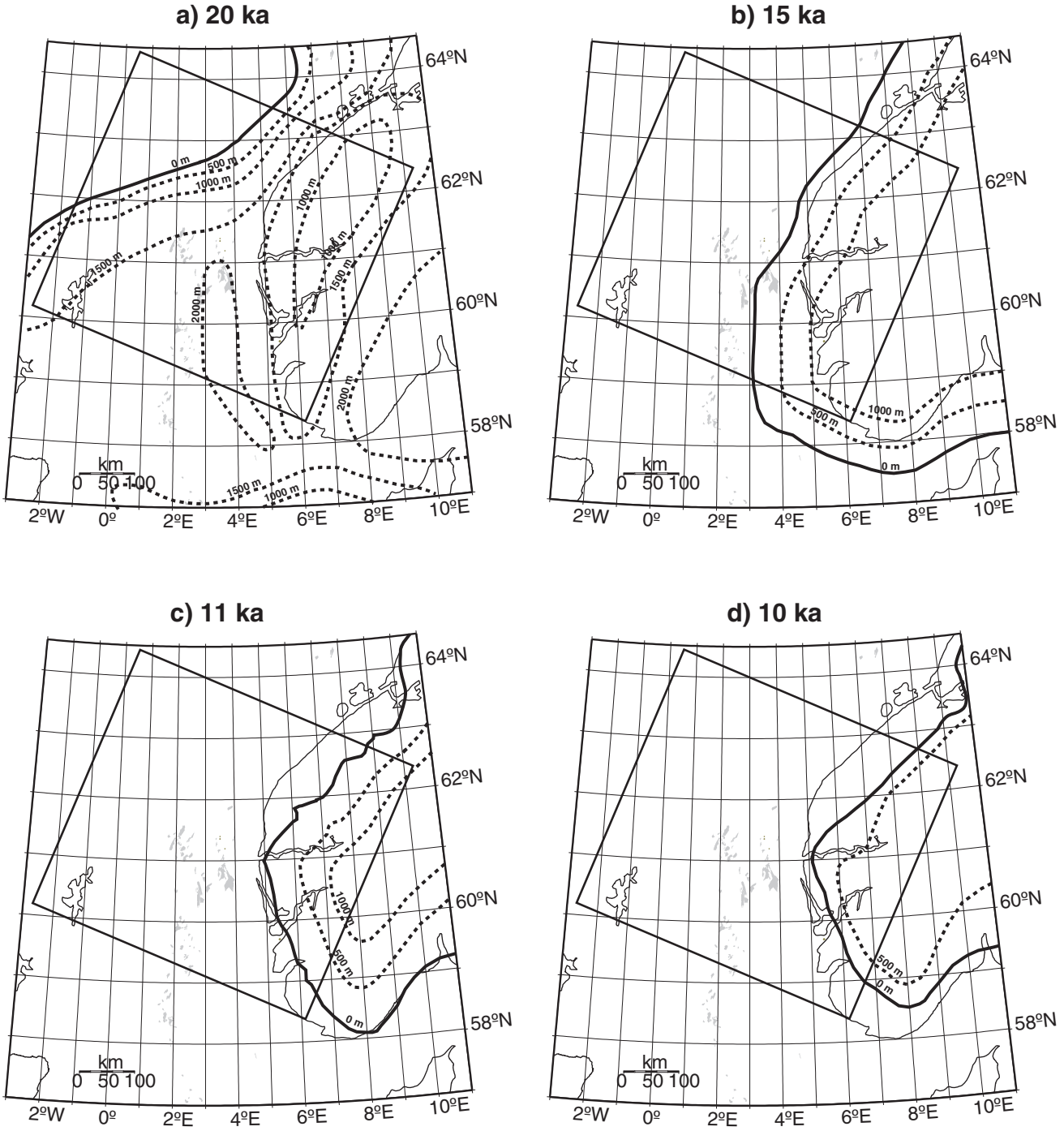

Figure 1. Extent and thickness of the modeled ice sheet for different stages of the North Sea model. (a) The figure shows the maximum ice sheet extent that existed at 20 ka. The ice extent at 15 ka (b) is the reference ice extent that is representative for most of the ice sheet's existence during the Pleistocene (Mangerud et al., 1979; Andersen, 1981; Lundqvist, 1986).

coast. Uplift following deglaciation could tilt hydrocarbon reservoirs and might cause leakage by changing the reservoir's spill point (Riis, 1992). Sales (1992) suggests that rapid subsidence and sedimentation caused by glacial erosion of the onshore areas affects hydrocarbon reservoirs by maximizing the cap rock seal integrity.

In this study, we investigate the effect of glaciation/deglaciation–induced stress changes on pore pressure and the effect of the temporally changing stress state on the leaking behavior of reservoir faults. An induced horizontal stress increase caused by lithospheric bending resulting from deglaciation can cause a pore pressure increase.

We assess the importance of this effect on the generation of the observed overpressures in parts of the northern North Sea (e.g., Caillet et al., 1991, Grollimund et al., 2001). Furthermore, the temporally changing stress field associated with ice growths and retreats can likely affect reservoir leakage by activating reservoir-bounding faults. Wiprut and Zoback (2002) show that leakage along potentially active faults affects several hydrocarbon reservoirs in the northern North Sea.

MODELING GLACIAL LOADING AND UNLOADING

The center model area is 250,000 km^2 (Figure 2), has a depth of 50 km, and is centered on the northern North Sea, which contains the most reliable stress data to constrain the model. To minimize boundary effects, a 300-km–wide zone (not shown in Figure 2), which shields the horizontally constrained boundaries from the center model area, surrounds the center model area. Figure 3a shows the model setup. The modeled upper crust is 20 km thick and has an elastic-plastic rheology. The real crustal structure in the investigated areas is not flat-layered as assumed in the models. In fact, the North Sea underwent rifting during Permian–Triassic and Jurassic–Early Cretaceous times (e.g., Færseth, 1996). We chose a simple crustal structure because we tried to keep the model as straightforward as possible to be able to investigate the sole impact of glaciation/deglaciation on the in-situ stress field. We assume linear elasticity for the elastic domain and perfect plasticity if the stress state exceeds the Mohr Coulomb failure criterion having a coefficient of friction (μ) of 0.6 in the absence of cohesion (Byerlee, 1978), which is a good representation of upper crustal rheology (Townend and Zoback, 2000).

Underneath the upper crust lies a Maxwell viscoelastic layer, representing the lower crust and the lithospheric mantle. The brittle upper crust–viscoelastic lower crust, and lower crust–lithospheric mantle interfaces are fully coupled, which means that displacement is uniform across these contacts. We include the asthenosphere by applying appropriate boundary conditions at the bottom of the lithosphere. More specifically, at each bottom node of the model, we apply a vertical force to account for isostasy, which allows the lithosphere to reach isostatic equilibrium after ice loading and to obtain lithospheric rebound following ice melting. We also apply a force that is proportional to the rate of vertical displacement to account for the viscous resistance of the asthenosphere.

Table 1 lists the rheological parameters used for the numerical models. The chosen values for density (ρ), Young's modulus (E), and Poisson's ratio (ν) are typical values for the corresponding lithospheric units, i.e., granites for the upper crust, gabbros for the lower crust, and peridotites for the lithospheric mantle. The viscosities (η) are based on estimates of a linearized power creep law for a wet Variscan continental crust (Strehlau and Meissner, 1987).

No lateral changes in crustal thickness and composition are included in the model, although Artyushkov (1973) has shown that the transition from continental to oceanic crust can affect crustal stresses. However, the continental slope is located at a distance of about 100 km from the area of interest and is unlikely to affect the model predictions.

The initial stress state before ice sheet growth is isotropic ($S_v = S_{Hmax} = S_{hmin}$), where S_v is the vertical stress, S_{hmin} is the minimum horizontal stress, and S_{Hmax} is the maximum horizontal stress. S_v is calculated with $\int \rho_{(z)} g dz$, where ρ is the density, g is gravity, and z is depth. McGarr (1988) suggests this isotropic stress state as a good estimate in the absence of tectonic forces. We exclude tectonic forces because the aim of this study is to assess the impact of short-term stress changes on reservoir faults. Tectonic forces caused by ridge push are expected to be constant during the time span considered here (2 m.y.). Furthermore, as shown below, the present-day stress predictions, in the absence of tectonic forces, approximate the observed stress field, which indicates that the impact of tectonic forces on the study area is small.

To include the ice sheet, we apply a distributed load corresponding to the weight of the ice at the surface of the model. The applied load varies spatially and temporally to account for changes in the ice sheet thickness. We obtained the necessary information on temporal and spatial ice thickness changes by compiling published data on ice sheet extents and thicknesses for different ice stages (Mangerud et al., 1979; Andersen, 1981; Lundqvist, 1986). The North Sea model includes four ice stages as illustrated in Figure 1. The ice extent at 15 ka can be regarded as representative for most of the ice sheet's existence during the Pleistocene, which is supported by the abundance of ice front features at the margin of the ice sheet (e.g., Andersen, 1981). Constrained by these observations, we model ice loading from 2 Ma with the 15-ka ice sheet extent (Figure 1b) and maintain this load until 110 ka (Figure 3b).

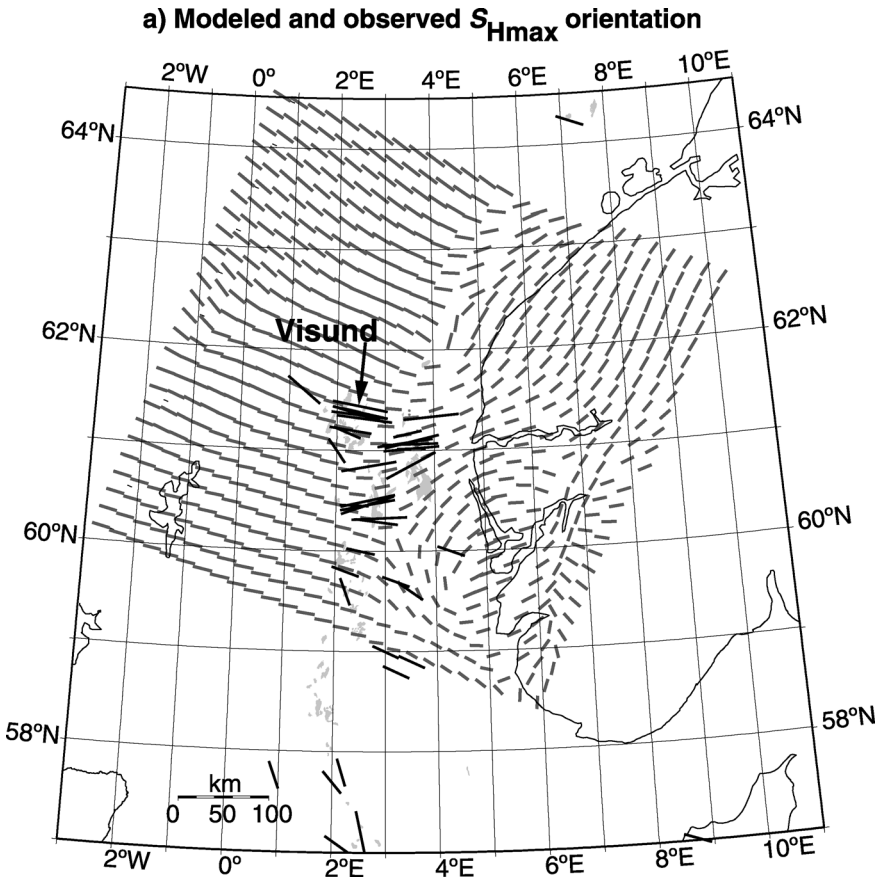

Figure 2. Comparison of modeled and observed present-day stress. In (a), the gray lines show the modeled results of S_{Hmax} which can be compared to the borehole measurements (black lines). (b) The figure shows the modeled S_{hmin}/S_v at a depth of 3000 m. (c) This figure shows observed S_{hmin}/S_v from leak-off tests for comparison. The model fits the observed stresses very well, suggesting that deglaciation causes the observed spatial stress variations.

Subsequently, we grow the ice sheet to its maximum extent and maintain this load during the Weichselian cold period between 110 and 20 ka but having three ice sheet melts, of which the most important one began approximately at 60 ka (Figure 3b). During the last 20 k.y., we gradually melt the ice sheet following the extents shown in Figure 1 until 9 ka when the entire ice sheet disappears and let the lithosphere equilibrate to present day.

THE PRESENT-DAY STRESS FIELD IN THE NORTHERN NORTH SEA

As a result of the procedure described above, the model provides the complete stress field at each point in time for the duration of the model until the present day, which is a requirement to estimate the impact of glacially induced stress changes on hydrocarbon migration. However, first, the model results need to be validated by comparing present-day stress predictions with in-situ stress measurements. The stress measurements consist of S_{Hmax} orientations from analyzing borehole breakouts and drilling-induced tensile fractures (Wiprut and Zoback, 2000a) and minimum horizontal stress measurements from borehole leak-off tests, normalized by the vertical stress (S_{hmin}/S_v) (Grollimund et al., 2001). These stress measurements cover the approximate uppermost 4 km of the upper crust and are compared to the model predictions at a depth of 3 km. The measured stress orientations and magnitudes are very consistent with depth, and the same is true for the model predictions in the approximate uppermost 10 km.

Generally, the model results agree with the borehole S_{Hmax} orientations (Figure 2a) and show that with deglaciation, S_{Hmax} orientations are nearly perpendicular to the ice sheet margins of the 15-ka ice extent at distances of greater than 100 km from the coast. Closer to the coast north of 61.5°N, the modeled S_{Hmax} orientations tend to align with the coastline. At a latitude of 61°N, the model reproduces the measured, roughly east-west–striking S_{Hmax} orientation and the smooth S_{Hmax} rotation from about 100° at 2.5°E to about 85° at 3.5°E. Further south, at around 60°N and 2.5°E, the model exactly matches the observed S_{Hmax} orientations. The model deviates from the measured S_{Hmax} orientation at 60°N and 4.5°E by almost 90°.

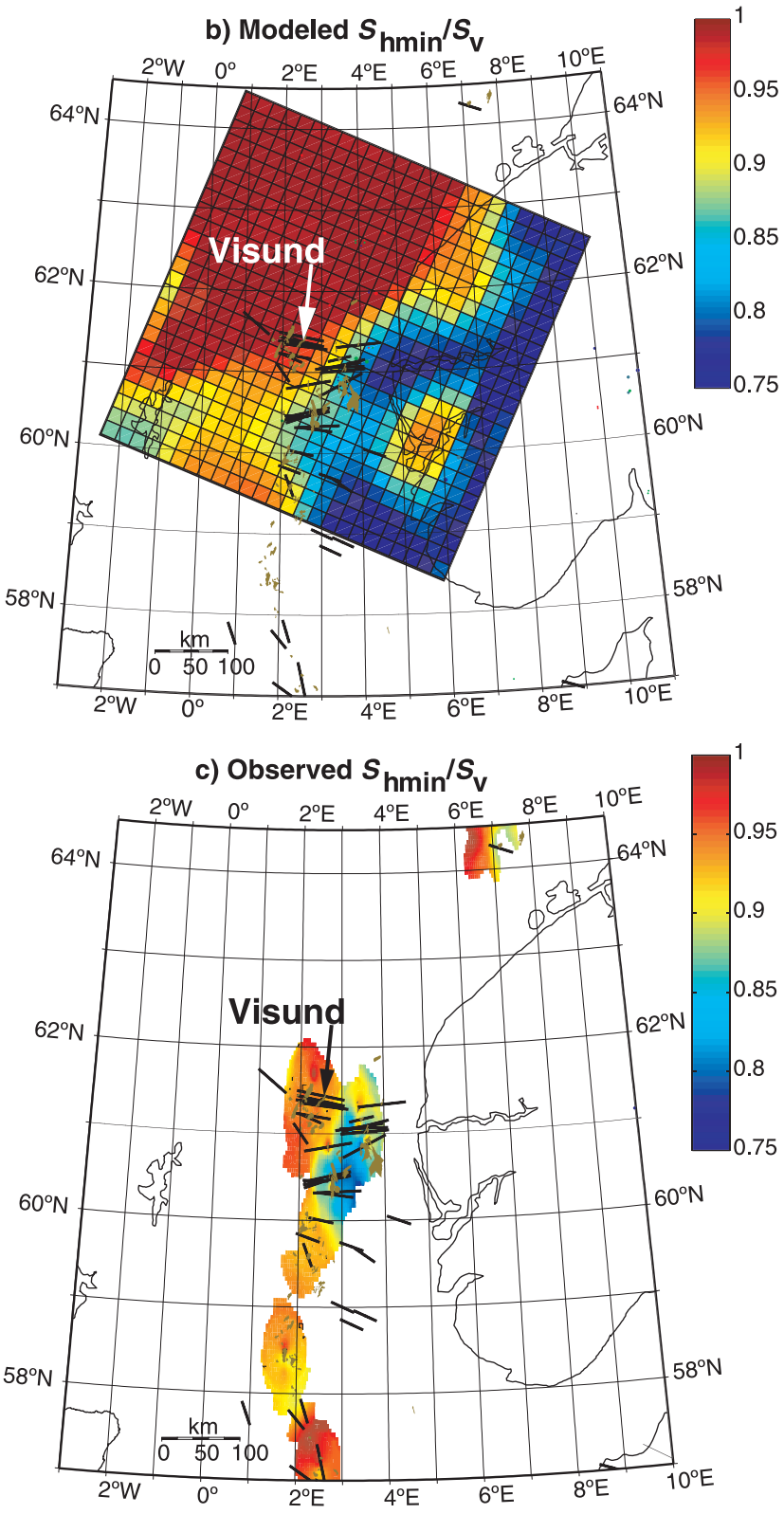

Figure 2. Continued.

However, this particular stress measurement is obtained from a breakout analysis using caliper logs. This kind of stress measurement has several potential error sources such as keyseating, and the measurement might reflect the orientation of the borehole instead of stress direction (Plumb and Hickman, 1985). Nevertheless, with few

Table 1. Rheological Parameters for the Model

Depth Unit	ρ (kg/m^3)	E (GPa)	ν	η (Pa s)	μ
Upper crust	2700	56	0.25	–	0.6
Lower crust	2900	71	0.25	10^{22}	–
Lithospheric mantle	3200	100	0.25	10^{23}	–

exceptions, the model fits the stress orientation data extremely well.

The computed and observed least horizontal stress fields are shown in (Figure 2b, c) for comparison. Note that the observed S_{hmin}/S_v in Figure 2c shows a marked decrease when approaching the coast. S_{hmin}/S_v measurements at distances of greater than 100 km from the coast are close to unity, indicating high horizontal stresses corresponding to a strike slip or even reverse faulting stress regime, whereas in close proximity of the coast (east of ~3°E), S_{hmin}/S_v appears to be significantly lower. The model accurately estimates the location and magnitude of the measured lateral S_{hmin}/S_v variations described above and shown in Figure 2c, thereby indicating that the processes contributing to the present-day stress field are adequately represented in the model. Obviously, other sources of stress contribute to the present-day stress field offshore Norway. For example, Gölke (1996) has shown that the large-scale tectonic forces resulting from ridge push significantly affect the regional stress field. It was the initial strategy of the work presented in this paper to investigate different combinations of stress sources to explain the measured present-day stress field in the northern North Sea. However, the good match between stress measurements and the model results, which are solely based on modeling glaciation/deglaciation, suggests that at least in the northern North Sea, where the studied oil fields are located, the stress field is adequately represented

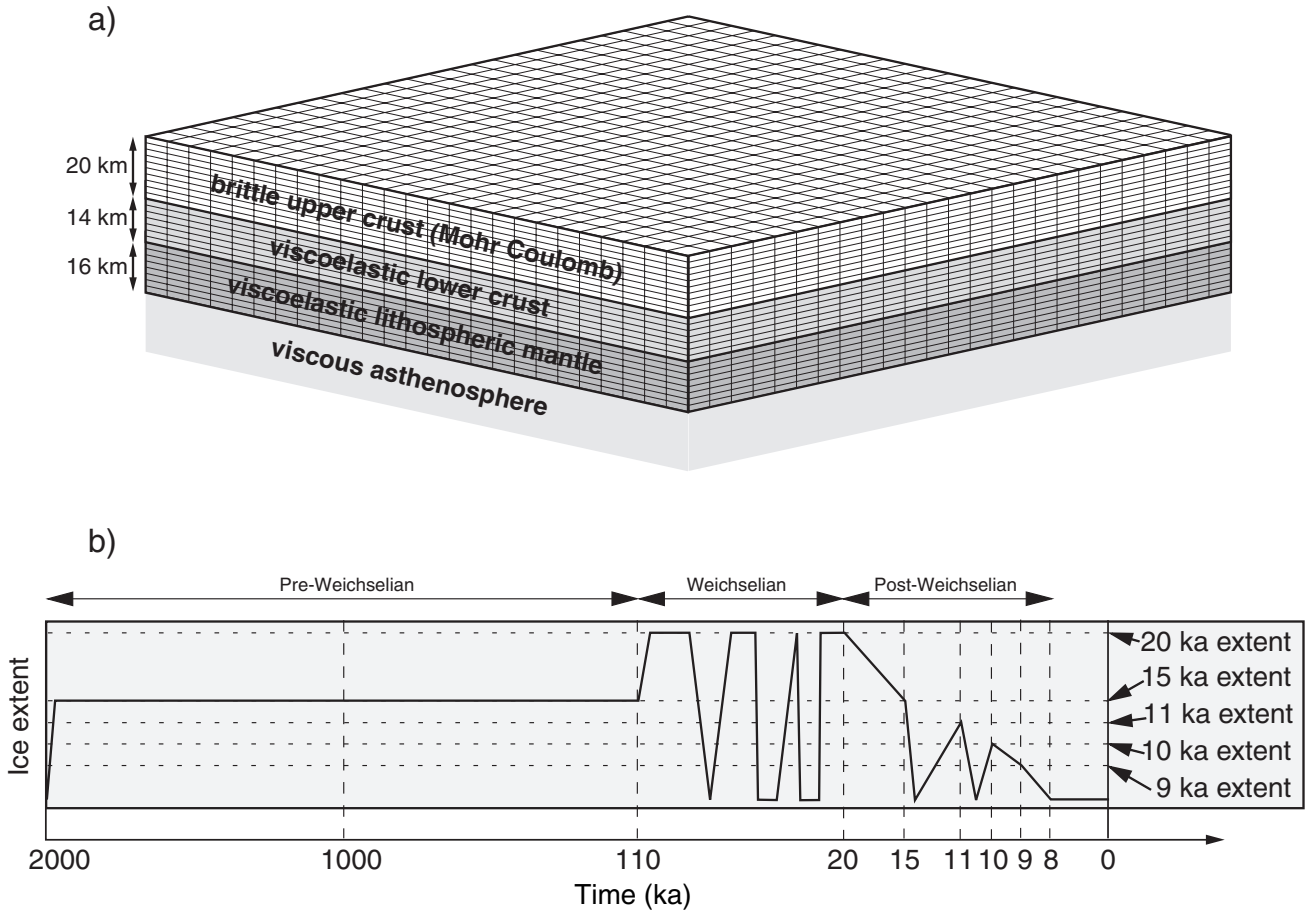

Figure 3. Setup of the numerical model. (a) The figure shows element sizes and modeled rheological layering of the lithosphere. In this figure, we only display the 15,625 elements in the center of the model, omitting the 5400 elements surrounding the area of interest. (b) Change of the modeled ice sheet extent with time.

despite the exclusion of other possible stress sources and complex crustal geometries.

THE EVOLUTION OF STRESS MAGNITUDES

By knowing that the modeled present-day stresses are consistent with the measured present-day stress field in the northern North Sea, we can assume that the model also provides some insight to the past evolution of the stress field. Otherwise, if the stress history was not appropriately included in the model, the present-day model results would not match with the stress measurements. In this section, we will illustrate the important components of the ''stress path'' that are responsible for the stress patterns observed today, to set the stage for investigating the impact of these changes on pore pressure and the leaking behavior of reservoir faults in the northern North Sea.

Figure 4 shows the modeled temporal changes of the maximum and minimum horizontal stresses normalized by the vertical stress (S_{Hmax}/S_v, and S_{hmin}/S_v), and similarly for the minimum horizontal stress (S_{hmin}/S_v) at a depth of 3000 m. At this shallow lithospheric depth, initial ice loading reduces the horizontal stress magnitudes in the vicinity of the ice front as a result of lithospheric flexure (Figure 4a, b). A forebulge starts to form off the Norwegian coast and consequently S_{Hmax}/S_v decreases to a value of 0.9. The ice-covered onshore areas experience a horizontal stress increase as a result of the bent lithosphere. The above-described stress pattern, as shown in Figure 4a and b, results from the immediate, elastic response of the lithosphere to ice loading as illustrated below Figure 4a and b.

Figure 4c and d show that with time, viscoelastic deformation significantly alters the horizontal stress magnitudes. The forebulge has moved toward the coast at 110 ka, and its shape is more pronounced, which is evidenced by low horizontal stresses ($S_{Hmax}/S_v \sim 0.8$, $S_{hmin}/S_v \sim 0.6$) near the Norwegian coast. On land, the horizontal stress magnitudes are lower than immediately after ice emplacement, because the viscoelastic lower lithosphere is extending under the weight of the overlying ice sheet.

Between 110 and 100 ka, the ice sheet grew to its maximum extent. The resulting horizontal stress magnitudes, shown in Figure 4e and f, are a mixture of the long-term ''imprint'' of the pre-Weichselian ice sheet and the elastic response to the newly grown Weichselian ice sheet. A zone of low S_{hmin}/S_v values forms near the new ice front, roughly between 62 and 63°N, but S_{Hmax}/S_v still tends to be higher beyond the former forebulge location. A laterally confined zone exhibiting high horizontal stress magnitudes forms in the vicinity of 61°N and 2°E. In this zone, lithospheric bending underneath the large ice sheet adds constructively to the already existing high stresses. Closer to the center of the large ice sheet, bending of the lithosphere is negligible, and the horizontal stresses remain almost unchanged. However, S_v increases drastically because of the overlying ice mass, which causes the S_{Hmax}/S_v and S_{hmin}/S_v ratios to drop significantly. For example, S_{Hmax}/S_v reaches values below 0.7 in southwestern Norway.

The modeled Weichselian ice sheet lasts for 80 k.y., during which time viscoelastic processes do not have enough time to significantly alter the lithosphere, so stress magnitudes remain almost unchanged. After the ice sheets melt back to the 15-ka extent, the stress magnitudes largely return to their pre-Weichselian (110 ka) values (Figure 4g, h) except at the outside perimeter of the Weichselian ice sheet where S_{Hmax} and S_{hmin} are permanently reduced. Areas that were covered by a significant ice pack during the Weichselian period exhibit increased S_{Hmax} and S_{hmin} magnitudes.

The ice front of the 10-ka extent was located between 20 and 50 km inland from the current coastline, which caused a decrease in the horizontal stress magnitudes along the coast, and in near-coastal offshore areas (Figure 4i, j). These areas were already exposed to relatively low horizontal stresses at 15 ka, so the effect of the 10-ka ice extent is even more pronounced. At distances of approximately 100 km inland of the present-day coastline, lithospheric flexure caused by loading of the 10-ka ice extent caused compression increasing the horizontal stresses.

During the last stages of ice melting, the horizontal stresses remained nearly unchanged except in areas that were still covered by ice at the 10-ka stage. This was the case for most onshore areas in southwestern Norway that were at least about 100 km inland from the present-day coastline (e.g., 60.5°N, 8°E on Figure 4i, j). In these places, ice melting caused an increase in S_{Hmax}/S_v and S_{hmin}/S_v, because the disappearing ice lowered S_v, instead of because of changes in S_{hmin} or S_{Hmax}. The sudden drop in vertical stress, while the horizontal stresses remained unchanged, resulted in a compressional stress state. In northern Norway and in northern Sweden, there is ample evidence for active thrust faulting, immediately following deglaciation (e.g., Olesen, 1988; Lagerbäck, 1990). The corresponding fault scarps were found at distances between 100 and 200 km from the current coastline. Our North Sea model estimates postglacial,

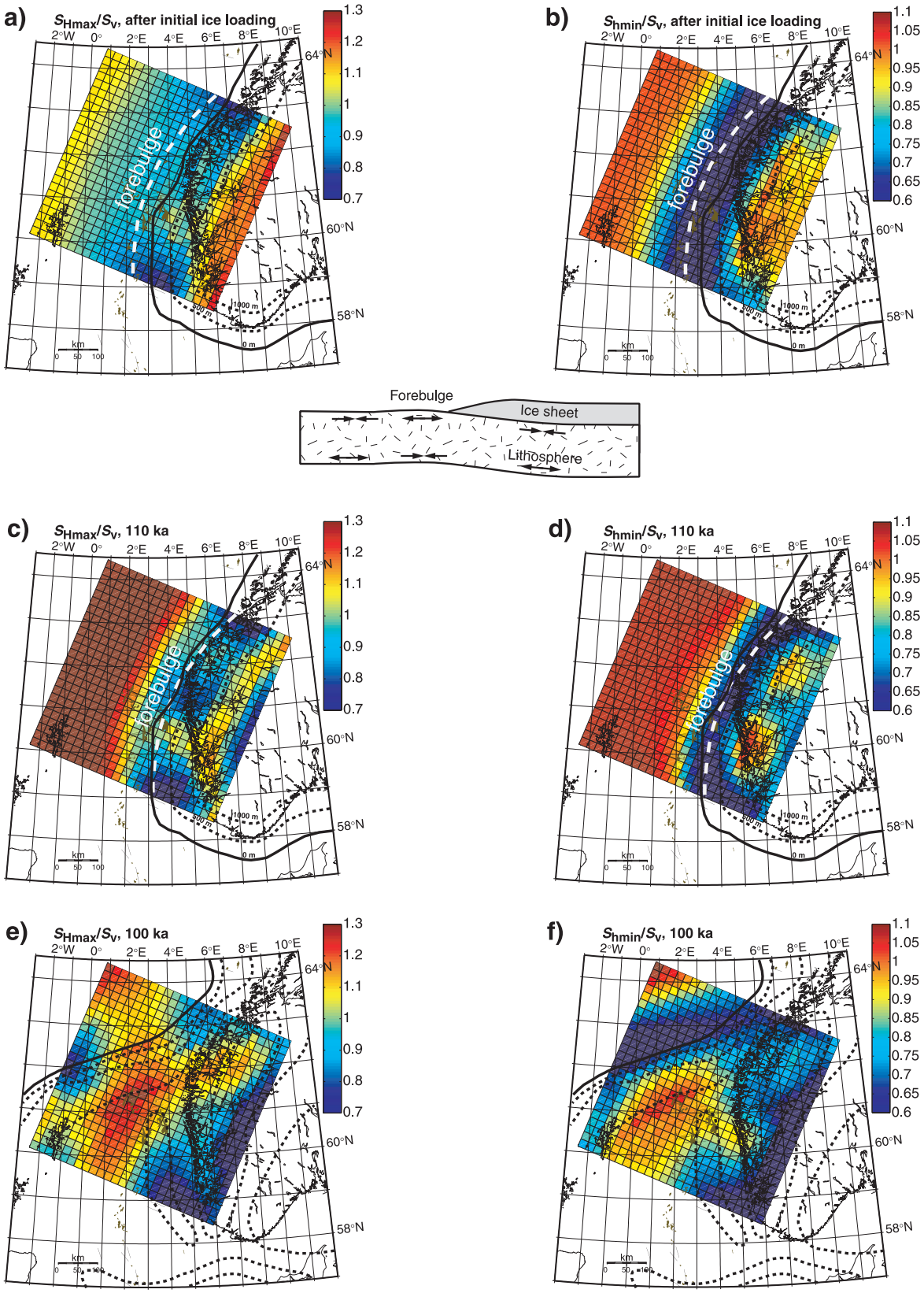

Figure 4. The figure shows the modeled spatial and temporal changes of S_{Hmax}/S_v, and S_{hmin}/S_v for the northern North Sea model at a depth of 3000 m. The extent of the ice sheet is also shown in each plot (solid black line), and the dashed lines indicate the ice sheet thickness in increments of 500 m.

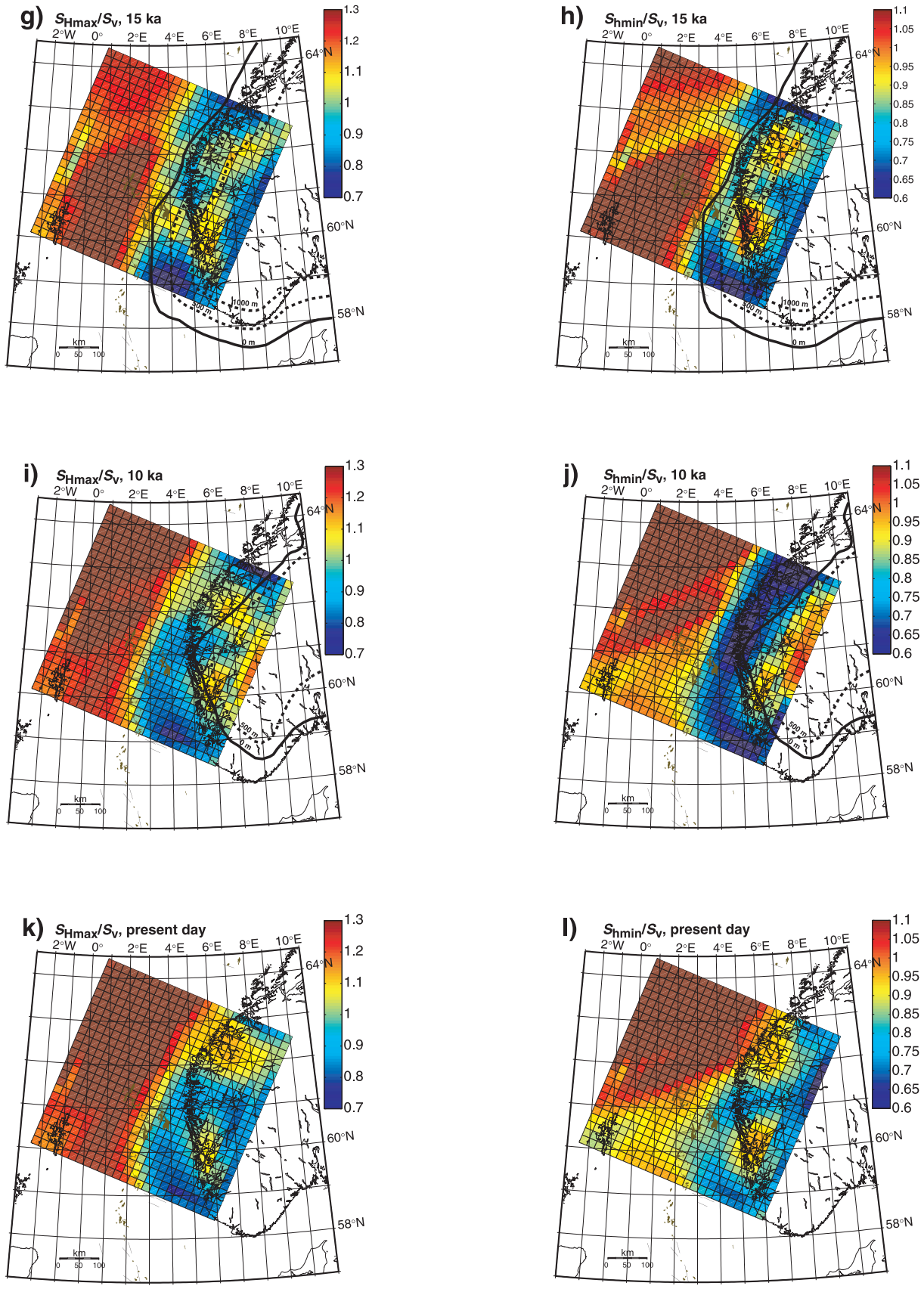

Figure 4. Continued.

thrust-faulting stress states at comparable distances from the coast. However, in most offshore areas, the present-day stress field is strike-slip faulting, as evidenced by S_{Hmax}/S_v values above 1 and S_{hmin}/S_v less than 1 (Figure 4k, l). Thus, present-day fault slip in the offshore areas is expected to be accommodated by steeply dipping strike-slip faults.

Postglacial lithospheric rebound gradually reduces these high horizontal stresses in the onshore areas and leads to the present-day stress patterns illustrated in Figures 4k, l, and 2. The present-day stress magnitudes are thus an artifact of the pre-Weichselian ice sheet having only a limited influence of the large, Weichselian ice sheet.

PREDICTED SEALING/LEAKING BEHAVIOR OF FAULTS

In this section, we will use the model of temporal stress changes to predict whether glacial growths and retreats contribute to leakage along reservoir faults in the northern North Sea. Our analysis is an extension of the findings of Barton et al. (1995), who suggested that critically stressed faults (i.e., oriented favorably for slipping in the current stress field) are conductive or permeable along their length, whereas noncritically stressed faults are impermeable. Wiprut and Zoback (2000b, 2002) showed that this concept appears to be valid for reservoir-bounding faults in the Visund field, and other fields in the northern North Sea. We utilize this concept to assess the sealing/leaking potential of reservoir-bounding faults in several fields over time.

To characterize a fault's sealing/leaking behavior at critical moments over the past 2 m.y., we calculate a Coulomb failure function (CFF) across the fault surface. The higher the CFF, the more likely it is for a fault to be active and conductive. To calculate CFF, we determine the fault normal vector (n) for the dip azimuth (θ) and dip angle (ϕ) of the fault, and calculate the fault's traction vector (t) for every model time step by simply multiplying the stress tensor (in the geographic coordinate system) by n. The resolved normal traction ($t_n = t \times n$) and the resolved shear traction ($t_s = |t - nt_n|$) on the fault plane yield the Mohr-Coulomb criterion for frictional sliding in the absence of cohesion:

$$\mathrm{CFF} = t_s - \mu(t_n - P_p) \qquad (1)$$

where μ is the friction coefficient. Equation 1 shows that an increase in P_p increases CFF and thus increases the chance for fault slip. We used the stress results obtained from the North Sea model along with fault orientations from some representative faults in the Visund, Field 3, and Field 1 fields (see Figure 2 for location of Visund, exact locations of the other fields are confidential). The fault orientations are obtained from depth-converted seismic data (Wiprut and Zoback, 2002) and are summarized in Table 2.

The fault orientations are average values that are representative for large parts of the analyzed faults at the modeled depth of 3000 m. As we only consider averaged fault orientations, our analysis only roughly estimates the potential for fault leakage.

The models assume hydrostatic pore pressure throughout the entire model duration. The pore pressure might have changed because of undercompaction, hydrocarbon maturation, or buoyancy effects associated with hydrocarbon columns, and triggered active faulting that could have caused leaking and in turn affected P_p (e.g., Finkbeiner et al., 2001). For these reasons, a more accurate fault analysis should be based on a coupled mechanical and fluid flow model accounting for changing P_p. However, such a coupled model is beyond the scope of this project. Consequently, our predictions of time-varying CFF serve only as a first-order estimate.

The most valuable information gained from this analysis is the relative change of CFF with time; the absolute CFF values are less certain. In Figures 5 and 6, we plot the difference between the calculated CFF and the calculated present-day CFF for an optimally oriented fault, which we define as ΔCFF. Positive values of ΔCFF indicate that a fault was most likely active.

Fault Analysis in Visund

The Visund field is located at 61.3°N and 2.5°E (see Figure 2 for location). At present, the Visund field is

Table 2. Fault Orientations Considered in the Analysis

Field	Fault	θ	ϕ
Visund	A north	102	21
Visund	A central	95	35
Visund	East west 3	68	21
Field 3	A	107	59
Field 3	B	278	54
Field 3	C	307	53

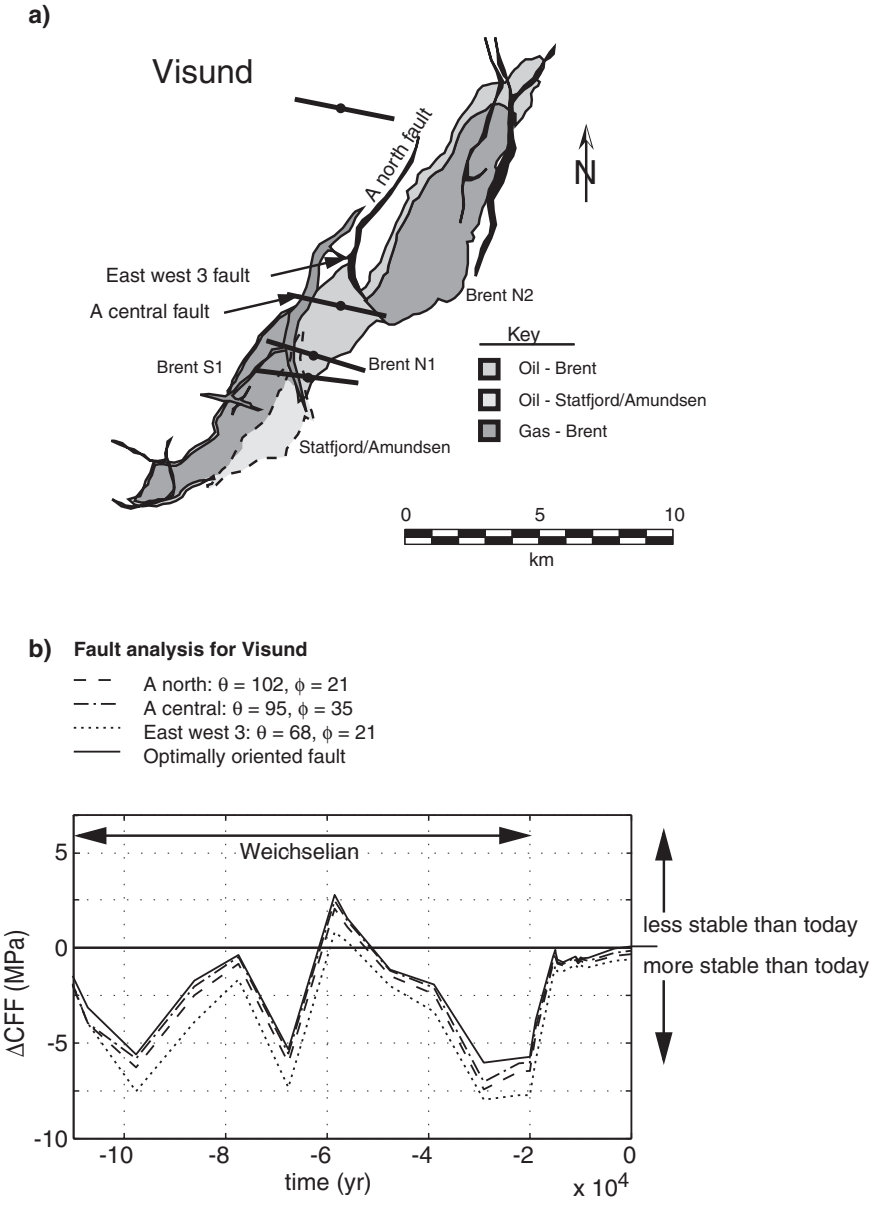

Figure 5. Fault leakage predictions for the Visund field. (a) Structural map of the Visund field showing the major faults and the reservoir extent. Inward pointing arrows indicate the S_{Hmax} orientations measured in the field. (b) Calculated ΔCFF for Visund during the last 110 k.y. The dashed lines show the calculated ΔCFF (calculated CFF referenced to present day) for the different faults, whereas the black solid line shows ΔCFF for an optimally oriented fault.

exposed to a strike or almost reverse faulting stress state, having S_{hmin} close to S_v and S_{Hmax}/S_v about 1.25 (Wiprut and Zoback, 2000a), which is consistent with our present-day model predictions. Figure 5a shows a map of the Visund field having the major reservoir faults, including the three faults considered in our analysis. These faults were formed during Permian–Triassic and Jurassic extension (Færseth, 1996). However, in the context of this study, fault age is not as important as fault orientation, which determines whether a fault is active under the given stress and pore pressure conditions. According to Wiprut and Zoback (2002), the A central and A north faults strike almost perpendicular to the present-day S_{Hmax} orientation (Figure 5a), dip at an angle of about 30°, and are therefore perfectly oriented for slip in the present-day strike-slip to thrust-faulting stress state. By carefully analyzing pore pressure and in-situ stress near the A central fault, Wiprut and Zoback find that these faults are presently close to being critically stressed. Furthermore, there is evidence for gas leakage above the A central fault (see Figure 5 for location), which lends support to the hypothesis of Barton et al. (1995) that critically stressed faults tend to be leaking. Thus, with the knowledge that perfectly oriented, critically stressed faults in the Visund field exist at present (ΔCFF = 0) and that these faults are leaking gas, it is fair to assume that positive ΔCFF in Figure 5b indicates past events of fault leakage.

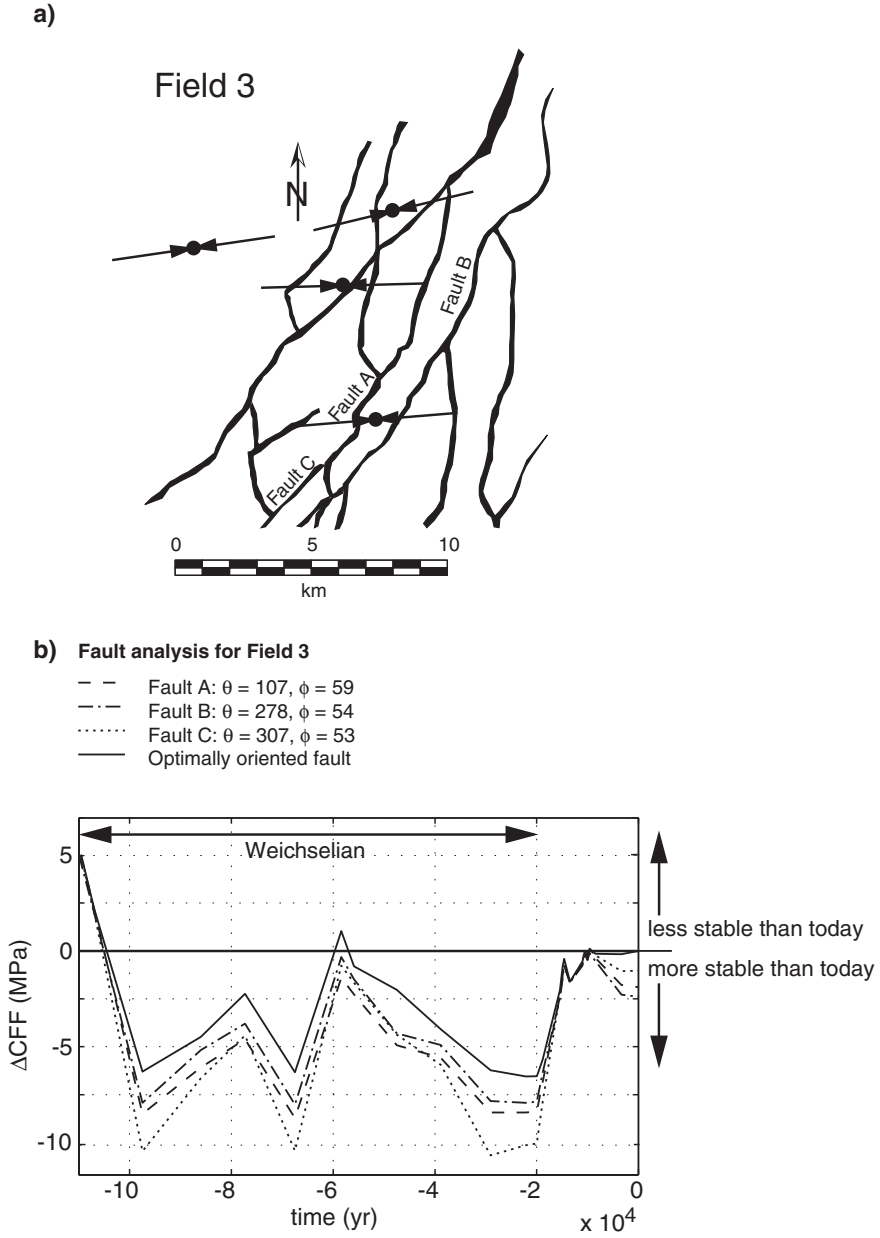

Figure 6. Fault leakage predictions for the Field 3 field. (a) Structural map of the Field 3 showing the major faults and the reservoir extent. Inward pointing arrows indicate the S_{Hmax} orientations measured in the field. (b) Calculated ΔCFF for Field 3 during the last 110 k.y. The dashed lines show the calculated ΔCFF (calculated CFF referenced to present day) for the different faults, while the black solid line shows ΔCFF for an optimally oriented fault.

In Figure 5b, we plot ΔCFF as a function of time, for three faults in the Visund field (A north, A central, East west 3) and a hypothetical, optimally oriented fault (solid black line). The plot shows the last 110 k.y., which corresponds to the Weichselian glaciations. During most of the Weichselian period, the ice sheet covered the Visund field and the stress state tended away from conditions favoring fault slip on the studied faults as indicated by low values of ΔCFF on Figure 5b. This is because the direct overburden of the ice sheet, which tends to prevent fault slip (e.g., Johnston, 1987), affected the stress state. Based on the findings of Barton et al. (1995), we therefore infer that reservoir faults tended to be impermeable during cold periods. Figure 5b shows positive ΔCFF before the Weichselian glaciation (110 ka), during a Weichselian interglacial 60 ka, and after the final melt of the large ice sheet about 15 ka, indicating that fault slip was triggered during these periods. Therefore, episodes of fault leakage are thought to have occurred during Weichselian interglacials and immediately following the meltdown of the large ice sheet at approximately 15 ka.

In conclusion, it is likely that the A central and A north faults are oriented favorably for slip in the past and by inference leaked at several times during Weichselian interglacials and after the final melt of the Weichselian

ice sheet. Several studies have found some evidence for Quaternary fault activity in the northern North Sea based on analysis of seismic data (e.g., Boe et al., 1992). However, it is very difficult to find conclusive evidence from seismic data because the accumulative fault offset associated with quaternary faulting is expected to be no more than 1–2 m.

Fault Analysis in Field 3

Figure 6a shows the major reservoir faults in Field 3. These faults generally are more oblique to the maximum horizontal stress than in Visund, and fault dip angles are higher (50–60°). In contrast to Visund, Field 3 shows no clear evidence for present-day leakage (Wiprut and Zoback, 2002). Some seismic cross sections appear to suggest gas chimneys above north-south–trending fault segments, but the evidence is inconclusive, which is in contrast with the clear evidence for gas leakage in Visund. The lack of leakage in Field 3 indicates that these faults are currently not critically stressed. A possible explanation for the apparent inactivity of faults in Field 3 is that they are not well oriented for slippage under the present-day stress field. As mentioned above, these faults have a much higher dip angle than faults in Visund (see Table 2) and are thus less prone to slip under the present-day strike-slip to thrust-faulting regime. Instead, faults in Field 3 would be optimally oriented for fault slip under normal faulting conditions having an S_{Hmax} orientation parallel to fault strike. In addition, Field 3 has lower pore pressures, which further reduces CFF and thus the likelihood for fault slippage.

Figure 6b shows that during the last 100 k.y., ΔCFF was always negative for the three faults analyzed in Field 3. Assuming that faults in Field 3 are currently inactive, as suggested above, the permanently negative ΔCFF implies that these faults have been inactive during the entire Weichselian. The only possible fault activation might have occurred during the relatively long interglacial at 60 ka, when ΔCFF was approaching negative values. Similar to the results for Visund, ΔCFF was very low during the maximum Weichselian ice sheet extents, which confirms earlier findings that the existence of the maximum ice extent serves to prevent fault slip, and thus, leakage events were unlikely.

In conclusion, the large Weichselian ice sheet suppressed active fault slip, but Weichselian interglacials might have possibly reactivated faults in Field 3. Weichselian faulting activity is much less probable in Field 3 than in Visund, which agrees with the lack of clear evidence for fault leakage.

CONCLUSIONS

We used the calculations of temporal stress changes resulting from glacial loading and unloading cycles to compare the potential fault reactivations to possible periods of leakage in the past. Although it is impossible to prove or disprove our estimates of past potential leakage, we can provide a rough idea on how the Pleistocene glaciations might have affected the slip of reservoir faults offshore Norway. The analysis suggests that all the investigated hydrocarbon reservoirs might have been exposed to fault slip and thus possibly leakage as a result of either glacial loading or unloading during their past. The maximum Weichselian ice extent prevented leakage throughout the northern North Sea, because the weight of the overlying ice sheet served to stabilize faults by increasing the isotropic part of the stress tensor. However, during Weichselian interglacials, the stress state changed such that leakage was promoted, especially in the vicinity of the ice margin. This finding implies that any hydrocarbon reservoir that is located in the vicinity of a former ice sheet margin may have been exposed to episodes of fault leakage, if the reservoir faults were preferably oriented. This study implies that in fields located just outside a former ice margin (e.g., Visund), the faults most prone for leakage are either striking parallel to the ice margin and have a small dip angle of about 30° (e.g., A central fault in Visund), or near-vertical having a strike angle that is about 60° different than the strike of the ice margin. These correspond to optimal fault orientations for slip under thrust to strike-slip faulting stress states. In fields that were previously covered by an ice sheet for long periods of time such as Field 3, fault leakage is most likely to occur in a normal to strike-slip faulting stress state. The corresponding fault orientations are either steeply dipping faults having a dip angle of about 60° and striking perpendicular to the ice front or near vertical faults having a strike that is at an approximately 60° angle to the ice front. The detailed assessment of fault leakage in a new hydrocarbon prospect should be based on a dedicated fault leakage study, which should include analysis of the local in-situ stress and pore pressure conditions. Nevertheless, the above conclusions can serve as a first-order assessment of glacially induced fault leakage.

REFERENCES CITED

Andersen, B. G., 1981, Late Weichselian ice sheets in Eurasia and Greenland, *in* G. H. Denton and T. J. Hughes, eds., The last great ice sheets: New York, Wiley, p. 1–65.

Artyushkov, E. V., 1973, Stresses in the lithosphere caused by crustal thickness inhomogeneities: Journal of Geophysical Research, v. 78, p. 7675–7708.

Barton, C. A., M. D. Zoback, and D. Moos, 1995, Fluid flow along potentially active faults in crystalline rock: Geology, v. 23, p. 683–686.

Boe, R., S. Sorensen, and M. Hovland, 1992, The Karmsundet Basin, SW Norway: stratigraphy, structure and neotectonic activity: Norsk Geologisk Tidsskrift, v. 72, p. 281–283.

Byerlee, J. D., 1978, Friction of rocks: Pure and Applied Geophysics, v. 116, p. 615–629.

Caillet, G., C. Sejourne, D. Grauls, and J. Arnaud, 1991, The hydrodynamics of the Snorre field area, offshore Norway: Terra Nova, v. 3, p. 180–194.

Færseth, R. B., 1996, Interaction of Permo-Triassic and Jurassic extensional fault-blocks during the development of the northern North Sea: Journal of the Geological Society, v. 153, p. 931–944.

Finkbeiner, T., M. D. Zoback, P. Flemings, and B. Stump, 2001, Stress, pore pressure, and dynamically constrained hydrocarbon columns in the South Eugene Island 330 field, northern Gulf of Mexico: AAPG Bulletin, v. 84, p. 1007–1031.

Gölke, M., 1996, Finite-element modelling of stress patterns along the mid-Norwegian continental margin, 62 degrees to 68 degrees N: Tectonophysics, v. 266, p. 33–53.

Grollimund, B., M. D. Zoback, D. Wiprut, and L. Arnesen, 2001, Stress orientation, pore pressure and least principal stress in the Norwegian sector of the North Sea: Petroleum Geoscience, v. 7, p. 173–180.

Johnston, A. C., 1987, Suppression of earthquakes by large continental ice sheets: Nature, v. 330, p. 467–469.

Lagerbäck, R., 1990, Late Quaternary faulting and paleoseismicity in northern Fennoscandia, with particular reference to the Lansjärv area, northern Sweden: Geologiska Föreningens i Stockholm Förhandlingar, v. 112, p. 333–354.

Lundqvist, J., 1986, Late Weichselian glaciation and deglaciation in Scandinavia: Quaternary Science Reviews, v. 5, p. 269–292.

Mangerud, J., E. Larsen, O. Longva, and E. Sonstegaard, 1979, Glacial history of western Norway 15,000–10,000 B.P.: Boreas, v. 8, p. 179–187.

McGarr, A., 1988, On the state of lithospheric stress in the absence of applied tectonic forces: Journal of Geophysical Research, v. 93, p. 13,609–13,617.

Olesen, O., 1988, The Stuoragurra Fault; evidence of neotectonics in the Precambrian of Finnmark, northern Norway: Norsk Geologisk Tidsskrift, v. 68, p. 107–118.

Plumb, R. A., and S. H. Hickman, 1985, Stress-induced borehole elongation: A comparison between the four-arm dipmeter and the borehole televiewer in the Auburn geothermal well: Journal of Geophysical Research, v. 90, p. 5513–5521.

Riis, F., 1992, Dating and measuring of erosion, uplift and subsidence in Norway and the Norwegian shelf in glacial periods: Norsk Geologisk Tidsskrift, v. 72, p. 325–331.

Sales, J. K., 1992, Uplift and subsidence of northwestern Europe: Possible causes and influence on hydrocarbon productivity: Norsk Geologisk Tidsskrift, v. 72, p. 253–258.

Strehlau, J., and R. Meissner, 1987, Estimation of crustal viscosities and shear stresses from an extrapolation of experimental steady state flow data, *in* K. Fuchs and C. Froidevaux, eds., Composition, structure and dynamics of the lithosphere-asthenosphere system: American Geophysical Union, Geodynamics Series 16, p. 69–87.

Townend, J., and M. D. Zoback, 2000, How faulting keeps the crust strong: Geology, v. 28, p. 399–402.

Wiprut, D., and M. D. Zoback, 2000a, Constraining the full stress tensor in the Visund field, Norwegian North Sea: application to wellbore stability and sand production: International Journal of Rock and Mineral Sciences, v. 37, p. 317–336.

Wiprut, D., and M. D. Zoback, 2000b, Fault reactivation and fluid flow along a previously dormant normal fault in the northern North Sea: Geology, v. 28, p. 595–598.

Wiprut, D., and M. D. Zoback, 2002, Fault reactivation, leakage potential, and hydrocarbon column heights in the northern North Sea, *in* A. P. Koestler and R. Hunsdale, eds., Hydrocarbon seal quantification: Amsterdam, Elsevier, p. 203–219.